

Scale-adaptive Wavelet-based Particle Detection in Microscopy Images

Oliver Greß¹, Birgit Möller¹, Nadine Stöhr², Stefan Hüttelmaier²,
Stefan Posch¹

¹Institute of Computer Science, Martin Luther University Halle-Wittenberg

²ZAMED, Martin Luther University Halle-Wittenberg

`oliver.gress@informatik.uni-halle.de`

Abstract. Stress granules and processing bodies play a major role in analysing the physiology of cells under various environmental conditions. We present a fully automatic approach to detect such particles in fluorescence labeled microscope images. The detection is based on scale-adaptive analysis of wavelet coefficients allowing for an accurate detection of particles with a large variety in size. Results on real images illustrate the appropriateness of our approach and proof high quality.

1 Introduction

Systems biology on the cellular level requires detailed analysis of different particles in cells like stress granules (SGs) and processing bodies (PBs). They are suggested to be dynamically linked to places of mRNA sorting and storage or degradation [1]. To understand and clarify the physiological roles of SGs and PBs, it is important to investigate the alterations of number, size, shape or contacts of these particles under different physiological conditions. Consequently the fully automatic detection of SGs and PBs is an essential tool to gain deeper insights into their biological role and function.

To detect spot-like particles, global and local thresholding techniques are still used in microscopy [2, 3]. Further techniques include h-dome transform followed by clustering [4]. Level set methods [5] on the other hand assume an approximately constant grey level shared by all target entities which typically does not hold for microscopy images. In [6, 7] a method to detect particles in microscopy images based on wavelet coefficients is proposed, but best-suited to detect particles with limited variation in size. Wavelet-based approaches are assumed to be superior to Fourier-based ones as their basis functions have local support.

We present an extension to the approach in [6, 7] aiming at the variable size of target entities by automatic scale-adaptation and test-based hypothesis selection.

2 Materials and Methods

The method in [6] is based on multi-scale analysis of wavelet coefficients. The original image $I_0(x, y)$ is recursively smoothed yielding images $I_1(x, y), \dots$,

$I_S(x, y)$. Wavelet coefficients $W_s(x, y)$ are derived as

$$W_s(x, y) = I_s(x, y) - I_{s-1}(x, y), \quad s \in \{1, \dots, S\} \quad (1)$$

For denoising, the amplitude-scale-invariant Bayes estimator [8] is applied, yielding adjusted coefficients $\tilde{W}_s(x, y)$. Features are represented by wavelet coefficients of adjacent scales. As the coefficients are correlated across scales due to the nature of the wavelet transform applied, adjacent scales are combined to a correlation image

$$c_{[a,b]}(x, y) = \prod_{s=a}^b \tilde{W}_s(x, y) \quad (2)$$

This correlation image is globally thresholded and the resulting connected components yield the final particles detected. The interval of scales $[a, b]$ used to correlate the wavelet coefficients defines the scales at which the particles of interest are represented. If all particles share the same characteristics, one interval is appropriate. In other cases one single interval either includes irrelevant scales or excludes important ones, in both cases often yielding incorrect particle size or shape, or missing particles.

To overcome these shortcomings we propose a new scale-adaptive technique which applies the wavelet-based segmentation to a set of – usually overlapping – intervals $[a_n, b_n]$, corresponding to different scales of particles. If for a target particle an appropriate interval is available, it is usually correctly detected in this interval. However, in many cases the particle is also found in adjacent intervals with incorrect size or shape (Fig. 1). This results in the necessity to select the correct one from overlapping and, thus, competing particle hypotheses. For this we propose an approach based on statistical hypothesis testing.

Typically hypotheses from the correlation image of a coarse scale result in larger regions than hypotheses from finer scales. Additionally, regions can be split up in finer scales due to the presence of multiple smaller particles or varying gray values inside larger particles.

We assemble competing hypotheses in trees whose nodes correspond to the particle regions detected in different intervals. The trees are build bottom-up

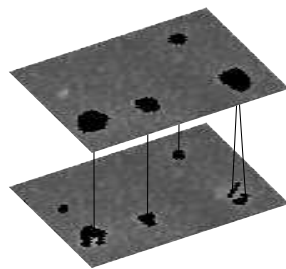


Fig. 1. Segmentation for two adjacent intervals (top: coarse, bottom: fine) and resulting hypotheses trees.

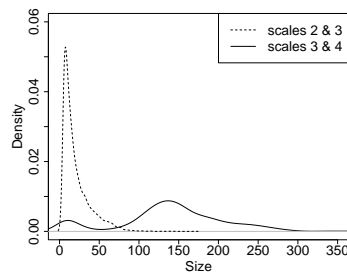


Fig. 2. Distribution of granule size detected in intervals $[a_1, b_1]$ and $[a_2, b_2]$.

starting with particle hypotheses from the finest scale. At each coarser level edges are inserted between a region and all overlapping regions of the next finer scale. Fig. 1 gives an example of the resulting hypotheses trees for two intervals.

In principle, two different regions at a coarse scale may both overlap with the same region at the next finer scale, destroying the tree characteristics of the hypothesis graph. However, this happened only once for the whole test data. Such constellations can for example be resolved using a simple criterion of largest overlap. The selection of one hypothesis out of several competing ones is accomplished using again a bottom-up procedure, starting from the fine scale leaves. Parent nodes are compared with their children and inferior nodes are deleted.

For comparison we employ the concept of meaningful events ([9]). This concept is tightly related to statistical hypothesis testing. In our case the null hypothesis H_0 models the case where no real particle is present at the location to be analyzed, rather a particle was detected due to noise or chance. To compute the likelihood $P(F_i | H_0)$ of a particle F_i detected under H_0 , the observations at all pixels are assumed to be pairwise independent

$$P(F_i | H_0) = \prod_{(x,y) \in F_i} P(C_{[a_n, b_n]}(x, y) = c_{[a_n, b_n]}(x, y) | H_0) \quad (3)$$

where $C_{[a_n, b_n]}(x, y)$ are random variables modelling the correlation value observed at position (x, y) . $P(C_{[a_n, b_n]}(x, y) = c_{[a_n, b_n]}(x, y) | H_0)$ is the probability to observe the value $c_{[a_n, b_n]}$ at location (x, y) due to noise. Following [10] we estimate $P(C_{[a_n, b_n]}(x, y) | H_0)$ as the discretized histogram of the complete correlation image for interval $[a_n, b_n]$.

The p-value $p(F_i)$ of F_i is the probability to observe a particle under the null hypothesis with correlation values at least as extreme as the ones of F_i . I.e., a particle with extremier values has at each pixel location in the correlation image a value larger than the one observed for F_i .

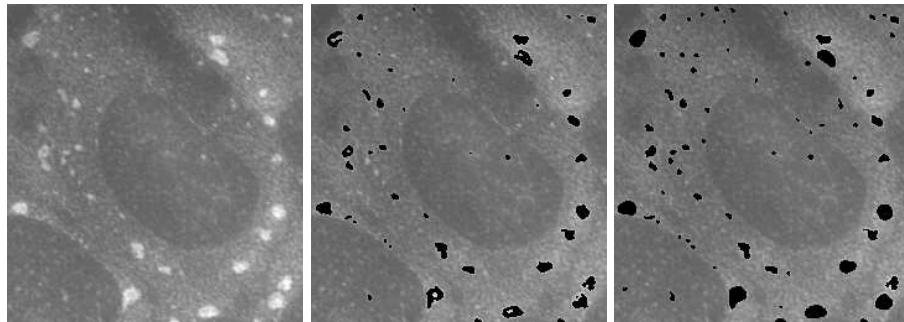


Fig. 3. Detection of stress granules. Left: Detail of image no. 8 with stress granules of varying sizes. Middle: Detection results using the method [6]. Right: Detection results using the scale-adaptive method (Image values scaled for visualization of results).

Still assuming independence of pixels this yields

$$p(F_i) = \prod_{(x,y) \in F_i} P(C_{[a_n, b_n]}(x, y) \geq c_{[a_n, b_n]}(x, y) | H_0) \quad (4)$$

We use this concept to compare a set of overlapping particle hypotheses to delete inferior nodes from the trees. We keep the particles with smallest p-value which consequently are assumed to be the ones most unlikely caused by chance. As p-values of particles with different size of support are compared, these raw p-values are normalized according to their support to allow fair comparison. In the case of multiple children their p-values are multiplied for comparison with the parent and we decide for F_i at the coarser scale if

$$p(F_i)^{\frac{1}{|F_i|}} < \prod_{\{k|F_k \text{ child of } F_i\}} p(F_k)^{\frac{1}{|F_k|}} \quad (5)$$

and for particles F_k on the finer scale otherwise.

3 Results

The proposed approach is tested on 10 microscope images of U2OS osteosarcoma cells stressed with sodium arsenate for one hour before fixation. SGs were labeled by immunostaining of ZBP1 in red, and for 5 images PBs were labeled by immunostaining of DCP1A in green.

For our application, two overlapping intervals of scale $[a_1, b_1] = [2, 3]$ and $[a_2, b_2] = [3, 4]$ have shown to be sufficient and will be used for the experiments reported in the following. Fig. 3 shows a detail of image no. 8 with fluorescently labeled SGs, and segmentation results for the method [6] with scales $[a, b] = [2, 4]$ and the proposed scale-adaptive method, respectively. For the scale-adaptive method the distribution of the size of granules detected in each of the scale intervals is depicted in Fig. 2. In analogy to Fig. 3, Fig. 4 gives segmentation results for PBs in a part of image no. 2.

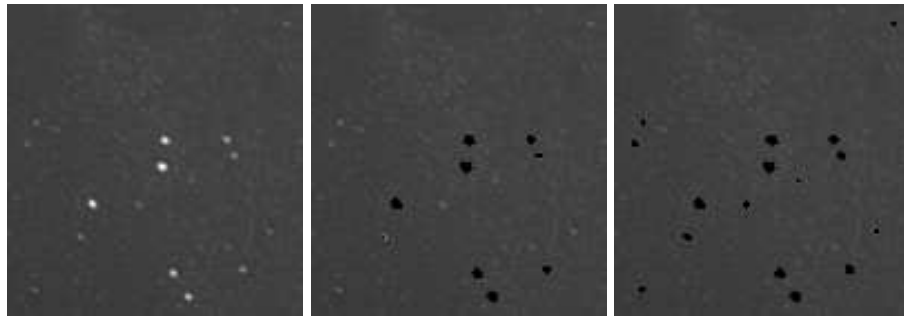


Fig. 4. Detection of processing bodies. Left: Detail of image no. 2 with processing bodies. Middle: Detection results using the method [6]. Right: Detection results using the scale-adaptive method. (Image values scaled for visualization of results).

4 Discussion

Stress granules show a large variety of different sizes and shapes. Using only one interval of wavelet coefficients as in [6] imposes the implicit constraint on similar shape and size for all granules. As can be seen from Fig. 3 (middle) this allows to detect a set of pronounced granules, however, misses several smaller granules and sometimes leads to incomplete segmentation for large granules, i.e. their shapes show deep convexities unusual for granules. In contrast, applying our new scale-adaptive approach based on selection of detection results from different scale intervals overcomes this problem. The detection is improved as detected granules cover a larger range of different scales and have more accurate contours (Fig. 3, right). The local adaptivity of our method shows also in Fig. 2. Detections from interval $[a_2, b_2]$ correspond mainly to large-sized granules, while small granules are detected predominantly in interval $[a_1, b_1]$.

Detection results for PBs also demonstrate the ability of our approach to automatically select features from the best scale. Compared to the results of method [6] our detection also includes PBs of less saliency (Fig. 4) avoiding the canceling effect of coarse scales. The variance in size among PBs is smaller than among SGs. Accordingly, a single fine-scale interval should be sufficient to detect the majority of PBs. Indeed, although intervals $[a_1, b_1]$ and $[a_2, b_2]$ are used for PBs detection, 99 % of the PBs are selected from interval $[a_1, b_1]$.

References

1. Kedersha N, Stoecklin G, Ayodele M, et al. Stress granules and processing bodies are dynamically linked sites of mRNP remodeling. *Cell Biol.* 2005;169(6):871–4.
2. Xavier J, Schnell A, Wuertz S, et al. Objective threshold selection procedure (OTS) for segmentation of scanning laser confocal microscope images. *J Microbiol Methods.* 2001;47(2):169.
3. Bolte S, Cordelieres FP. A guided tour into subcellular colocalization analysis in light microscopy. *J Microsc.* 2006;224(3):213–32.
4. Smal I, Niessen W, Meijering E. A new detection scheme for multiple object tracking in fluorescence microscopy by joint probabilistic data association filtering. In: *Proc IEEE ISBI; 2008.* p. 264–7.
5. Chan TF, Vese LA. Active contours without edges. *IEEE Trans Image Process.* 2001;10(2):266–77.
6. Olivo-Marin JC. Extraction of spots in biological images using multiscale products. *Pattern Recognit.* 2002;35(9):1989–96.
7. Dufour A, Meas-Yedid V, Grassart A, et al. Automated quantification of cell endocytosis using active contours and wavelets. In: *Proc ICPR; 2008.*
8. Figueiredo MAT, Nowak RD. Wavelet-based image estimation: an empirical Bayes approach using Jeffrey’s noninformative prior. *IEEE Trans Image Process.* 2001;10(9):1322–31.
9. Desolneux A, Moisan L, Morel JM. A grouping principle and four applications. *IEEE Trans Pattern Anal Mach Intell.* 2003;25(4):508–13.
10. Desolneux A, Moisan L, Morel JM. Edge detection by helmholtz principle. *J Math Imaging Vis.* 2001;14(3):271–84.